CrossMark

Assessment of Fire Engineering Design Correlations Used to Describe the Geometry and Thermal Characteristics of Externally Venting Flames

Eleni K. Asimakopoulou [ID], Dionysios I. Kolaitis* [ID] and Maria A. Founti, *Laboratory of Heterogeneous Mixtures and Combustion Systems, Thermal Engineering Section, School of Mechanical Engineering, National Technical University of Athens, Heroon Polytechneiou St. 9, Polytechneioupoli Zografou, Athens 15780, Greece*

Abstract. Externally venting flames (EVF) may emerge through openings in fully developed under-ventilated compartment fires, significantly increasing the risk of fire spreading to higher floors or adjacent buildings. Several fire engineering correlations have been developed, aiming to describe the main characteristics of EVF that affect the fire safety design aspects of a building, such as EVF geometry, EVF centreline temperature and EVF-induced heat flux to the façade elements. This work is motivated by recent literature reports suggesting that existing correlations, proposed in fire safety design guidelines (e.g. Eurocodes), cannot describe with sufficient accuracy the characteristics of EVF under realistic fire conditions. In this context, a wide range of EVF correlations are comparatively assessed and evaluated. Quantification of their predictive capabilities is achieved by means of comparison with measurements obtained in 30 different large-scale compartment-façade fire experiments, covering a broad range of heat release rates (2.8 MW to 10.3 MW), ventilation factor values ($2.6 \text{ m}^{5/2}$ to $11.53 \text{ m}^{5/2}$) and ventilation conditions (no forced draught, forced draught). A detailed analysis of the obtained results and the respective errors corroborates the fact that many correlations significantly under-predict critical physical parameters, thus resulting in reduced (non-conservative) fire safety levels. The effect of commonly used assumptions (e.g. EVF envelope shape or model parameters for convective and radiative heat transfer calculations) on the accuracy of the predicted values is determined, aiming to highlight the potential to improve the fire engineering design correlations currently available.

---

* Correspondence should be addressed to: Dionysios I. Kolaitis, E-mail: dkol@central.ntua.gr

Nomenclature

Symbol (Units – Value)	Description
A_0 (m^2)	Opening area
A_v (m^2)	Total area of vertical openings on all walls of the compartment
c (4.67)	Empirical factor (Eq. 19)
C_p (1005 J/kg K)	Specific heat of air at ambient conditions
D_v (m)	Effective diameter of the opening
d_{eq} (m)	Characteristic length scale of an external structural element
E_b (kW/m^2)	Black body emissive power
g (9.81 m/s^2)	Gravitational acceleration
H_0 (m)	Opening height
H_u (13,100 kJ/kg O$_2$)	Heat release of cellulosic fuels for each kilogram of oxygen consumed
h_{eq} (m)	Weighted average of openings heights on all walls
k (m^{-1})	Extinction coefficient
k_{fuel} (m^{-1})	Extinction coefficient for the combustion products of a specific fuel
$L_{L\_0.05}$ (m)	Flame height at the "continuous flame" (5% flame intermittency limit)
$L_{L\_0.50}$ (m)	Flame height at the "intermittent flame" (50% flame intermittency limit)
$L_{L\_0.95}$ (m)	Flame height at the "far-field flame" (95% flame intermittency limit)
L_L (m)	Height of EVF
L_H (m)	Projection of EVF
L_f (m)	Flame length
l (–)	Characteristic length scale (Eq. 9)
l_x (m)	Length along the EVF centerline, originating at the opening
$\dot{m}_a$ (kg/s)	Air mass flow rate (entering the fire compartment)
$\dot{m}_f$ (kg/s)	Fuel mass flow rate
$\dot{m}_{O_2}$ (kg/s)	Oxygen mass flow rate
$\dot{m}_g$ (kg)	Mass flow rate of unburnt gases venting outside the fire compartment
$\dot{Q}$ (MW)	Heat Release Rate
$\dot{Q}_{ex}$ (MW)	Excess Heat Release Rate
$\dot{Q}_{in}$ (MW)	Average heat release rate at the interior of the fire compartment
$\dot{q}''$ (W/m^2)	Heat flux
$\dot{q}''_{conv}$ (W/m^2)	Convective heat flux
$\dot{q}''_{rad}$ (W/m^2)	Radiative heat flux
r (–)	Fuel-to-oxygen stoichiometric mass ratio
r' (–)	Oxygen-to-fuel stoichiometric mass ratio
r_0 (m)	Equivalent radius of the opening
T_z (K)	EVF centerline temperature in relation to height from the opening lintel
T_{amb} (K)	Ambient temperature
T_f (K)	"Effective" flame temperature
T_0 (K)	Temperature at the center of the opening
T_{wall} (K)	Facade wall temperature
V (m/s)	External wind speed
$\dot{V}$ (m^3/s)	Air volumetric flow rate
W_0 (m)	Opening width
w_f (m)	EVF width
w_t (m)	Sum of opening widths on all walls of the fire compartment
w_d (m)	Distance to any other opening
$Y_{O_2,air}$ (0.232)	Oxygen mass fraction in ambient air
z (m)	Height above the opening lintel
Z_n (m)	Height of the neutral plane

Greek letters

a_c (W/m^{2}K)	Convective heat transfer coefficient
ΔT_m (K)	Plume centerline temperature rise above ambient
ε (−)	Emissivity
ε_z (−)	Local emissivity of the flame
λ (m)	Flame thickness
ρ_{amb} (1.204 kg/m^3)	Air density at ambient conditions
$\rho_{500^\circ C}$ (0.45 kg/m^3)	Air density at 500°C
σ (5.67 × 10^{-8} kg/s^{3}K^4)	Stefan Boltzmann constant
φ_f (−)	Configuration factor (radiation from fire through the opening)
φ_z (−)	Configuration factor (radiation from EVF)

Abbreviations

EVF	Externally venting flames
FD	Forced draught
GER	Global equivalence ratio
HRR	Heat release rate
NoFD	No forced draught
VF	Ventilation factor

1. Introduction

In a fully developed, under-ventilated compartment fire, flames may spill out of external openings (e.g. windows) in the case of glazing failure. It is well established that Externally Venting Flames (EVF) significantly increase the risk of fire spreading to higher floors or adjacent buildings [1, 2]. New façade design concepts and construction materials constantly challenge the established fire safety solutions. For instance, due to the ever stricter requirements for building energy performance, there is a growing trend in installing thermal insulation materials, that are usually flammable (e.g. polystyrene-based), on building façades. This energy saving practice is adversely affecting the building's fire safety characteristics related to EVF. However, the majority of current fire safety codes, worldwide, lack specific methodologies to evaluate the risks associated with EVF. The increasing occurrence of EVF events in high rise buildings, resulting in a large number of casualties, structural damage and property loss [1, 3, 4], renders the need to improve design guidelines for EVF and façade fires an urgent priority.

In order to effectively act towards EVF prevention and mitigation of external fire spread, it is essential to understand the nature of the fundamental physical phenomena affecting EVF. Research on EVF, focused on identifying the main physical parameters governing the compartment fire dynamics and the necessary conditions for an EVF to develop, commenced in the early 1960s by Yokoi [5] and was followed later on by other researchers [6–9]. The main findings of these research efforts, regarding EVF description and its impact on facades, were gradually incorporated in fire safety codes and design guidelines. However, addressing EVF related risks is still far from adequate. For instance, in the Eurocode design guidelines [10], there are only coincidental references to risks associated with EVF

(i.e. protection of steel [11] and timber external building elements [12]); fire spreading due to combustible façade materials is not addressed at all.

This work is motivated by an increasing number of reports [13–17] suggesting that existing engineering design methodologies cannot describe with sufficient accuracy the characteristics of EVF under realistic fire conditions. The main scope of this paper is to assess a range of fire engineering correlations currently implemented in guidelines used for the design of external building elements [2, 16, 18, 19] and to investigate the challenges associated with the proper application of each model. Correlations used to describe the geometric and thermal characteristics of EVF, as well as methodologies for the evaluation of the EVF-induced thermal exposure of building facades, are evaluated. The predictive accuracy of each model is assessed through comparison with available data from 30 large scale compartment-facade fire experiments, for a large variety of fuel loads and ventilation conditions. A statistical analysis is performed and the parameters that have a major effect on calculation results are discussed in detail.

2. Externally Venting Flames in Compartment Fires

2.1. Characteristics of Externally Venting Flames

Externally Venting Flames are essentially flames that traverse an opening of the fire compartment and emerge to the ambient environment [7, 20]. The basic compartment fire phenomena and resulting EVF shapes, as described in the majority of the currently available design guidelines, e.g. the Eurocode [10], are illustrated in Figure 1. Fire ventilation mode, geometric characteristics of the fire compartment and prevailing ventilation conditions are known to have a significant effect on EVF development [10, 13–15, 21, 22].
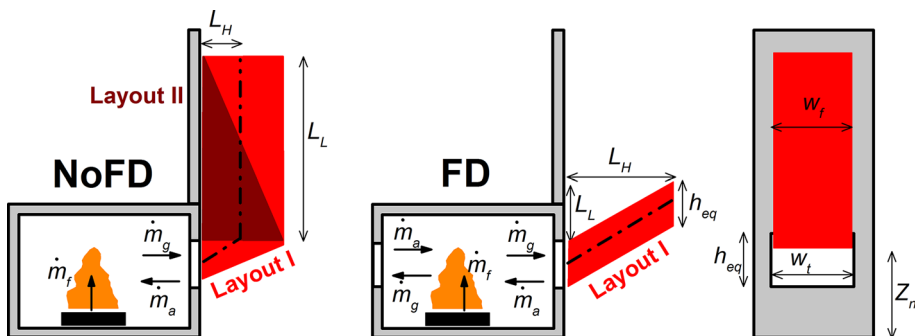
Figure 1. Schematic of the general EVF shape assumed in engineering correlations for NoFD (*left*) and FD (*middle*) conditions; front view of the compartment-façade configuration (*right*).

2.1.1. Fire Ventilation Modes Several phenomena are known to govern compartment fire dynamics [23]. During the initial stages of fire development, combustion is limited at the interior of the fire compartment. Incoming air enters the compartment at a specific mass flow rate ($\dot{m}_a$) through the lower part of the opening, whereas hot, vitiated, gases ($\dot{m}_g$) exit through the upper part of the opening. Depending on the size of the compartment and the fire load, it is possible to have a fire plume that cannot be contained within the compartment; in this case flames are ejected through the opening, due to the expansion of the buoyant turbulent flame at the exterior of the compartment [23]. In addition, under oxygen deficiency conditions (ventilation-controlled fire), external burning of fuel rich gases leaving the compartment may also occur, further sustaining EVF development [2, 6, 7, 23].

During the fire growth stage, the fire may be either fuel- or ventilation-controlled, depending on the ventilation conditions, heat release rate and geometry of the opening. In the fully-developed fire stage the fire gas temperature reaches its maximum value and remains practically constant; in this case, the fire is usually ventilation-controlled, unless there are uncommonly large openings or a limited fuel surface area [23, 24]. Due to differences in the severity of a fire event during the fuel- and ventilation-controlled stages, it is important to distinguish between the two cases [23–25]. There are several methodologies currently employed to characterise and distinguish between the two fire ventilation modes. Conservative formulations based on simplified energy balance calculations and experiments on fire compartments (e.g. [7, 8, 21, 25, 26]), tend to accurately describe most ventilation-controlled fires; however their accuracy is limited in most fire events involving realistic fuel loads [23].

A useful quantity to distinguish between the two fire ventilation modes is the Global Equivalence Ratio (*GER* or Φ) [23], expressed in Eq. (1) as the ratio of the fuel mass flow rate ($\dot{m}_f$) to the oxygen mass flow rate entering the compartment ($\dot{m}_{O_2}$), divided by the fuel-to-oxygen stoichiometric mass ratio (*r*) [23, 26]. The mass flow rate of the oxygen entering the compartment can be estimated using an empirical correlation, Eq. (2) [23, 26]. The oxygen mass fraction in air, $Y_{O_2,air}$, is assumed to be equal to 0.232. When the value of *GER* exceeds unity the fire is considered as ventilation-controlled (under-ventilated); when *GER* is less than one, the fire is regarded as fuel-controlled (well-ventilated).

$$GER = \frac{\dot{m}_f}{r \cdot \dot{m}_{O_2}} \tag{1}$$

$$\dot{m}_{O_2} = \begin{cases} 0.5\, Y_{O_2,air} A_0 \sqrt{H_0}, & \text{natural ventilation} \\ 0.23\, \rho_{\text{amb}}\, \dot{V}, & \text{mechanical ventilation} \end{cases} \tag{2}$$

The equivalence ratio can alternatevily be estimated using Eq. (3), where the oxygen-to-fuel stoichiometric mass ratio (*r'*) is employed [23]. This formulation enables the direct use of the oxygen-to-fuel stoichiometric mass ratio values that

are available for a large variety of commonly used fuels. The fuel combustion rate ($\dot{m}_f$) and the air mass flow rate entering the compartment ($\dot{m}_a$) can be estimated using Eqs. (4) and (5), respectively. The heat release rate ($\dot{Q}$) is typically estimated experimentally, using a cone calorimeter. The air mass flow rate entering the compartment ($\dot{m}_a$) is considered to be independent of temperature (above 150°C) and can be estimated using the ventilation factor, $A_0(H_0)^{1/2}$ [23]. Equation (5) is derived by applying the Bernoulli equation to the air flow into the fire compartment through a single opening; a 0.52 constant is used when post-flashover conditions prevail.

$$GER = \frac{\dot{m}_f \cdot r'}{\dot{m}_a \cdot Y_{O_2,air}} \tag{3}$$

$$\dot{m}_f = \frac{\dot{Q}}{H_u} \tag{4}$$

$$\dot{m}_a = 0.52 \cdot A_0 \sqrt{H_0} \tag{5}$$

2.1.2. Effect of Forced Draught Conditions EVF exhibit significantly different characteristics depending on the number and position of openings in the fire compartment [10, 21]. When openings are present on one side only of the fire compartment, No Forced Draught (NoFD) conditions are established [10]. In this case, the openings (e.g. window or door) are the only source of air supply to the fire and either fuel- or ventilation-controlled conditions may characterize the fire behaviour. On the other hand, when there are openings on opposite sides of the fire compartment or additional air is being fed to the fire from another source (e.g. mechanical ventilation), forced draught (FD) conditions can be established [10]. In this case, due to adequate ventilation levels, fuel-controlled conditions usually prevail. Suggested fire engineering design correlations are identical in both cases; however, the heat release rate values used in the calculations may differ. Heat release rate in fuel-controlled fire conditions is mainly affected by the free burning (open air) fire duration, whereas in ventilation-controlled conditions, the heat release rate depends on the compartment and opening geometry [10, 21]. Both NoFD [9, 13, 14, 27, 28] and FD conditions [13–15, 27, 28] are investigated in this work, since limited research has been conducted on the latter case (FD conditions), where the increased air flow into the compartment may significantly alter the fire characteristics [13–15, 29], due to the increased combustion rate (Figure 1).

The main EVF geometric characteristics under both NoFD and FD ventilation conditions are depicted in Figure 1. Two different layouts for the EVF shape, one corresponding to a constant flame thickness (Layout I) and another pertaining to triangular-shaped flame (Layout II), are illustrated in the NoFD conditions schematic (Figure 1, left). In Layout I, the flame is assumed to project from the fire

compartment at an angle of 45° to the horizontal [10, 15, 21]; it then bends upwards, exhibiting a constant flame thickness. In Layout II, the EVF assumes a triangular form, originating at the lintel of the opening. Under FD conditions, the jet-like EVF is considered to vent away from the façade through the entire height of the opening, exhibiting a constant flame thickness (Figure 1, middle); effects of buoyancy and mixing are not significant in this case [10, 15, 30]. Fuel combustion rate ($\dot{m}_f$), air mass flow rate entering the compartment ($\dot{m}_a$) and unburnt volatiles and smoke mass flow rate exiting the compartment ($\dot{m}_g$) are also depicted in Figure 1, for both ventilation conditions. In the front view of the façade (Figure 1, right), EVF width (w_f) and opening dimensions (h_{eq} and w_t) are illustrated, along with the characteristic height of the neutral plane (z_n). Although the geometric boundaries (shape) of the EVF envelope change dynamically, it is common practice for fire engineering design correlations to assume a uniform shape, defined via flame height (L_L), projection (L_H) and width (w_f) [10, 13–15, 21]; the EVF width (w_f) is usually assumed to be equal to the opening width (w_t) [10, 21].

Although much attention has been drawn on the impact of the opening geometry [5, 9, 19] on the EVF, scarce experimental data exist [5, 21, 31] regarding the effect of ventilation and external side wind on the EVF geometric characteristics; even in these cases only a few of them employ real scale experiments [5, 21]. It is well established that high and narrow openings produce a larger EVF, projecting in a greater distance from the surface of the adjacent facade wall, whereas wider and low openings create a shorter EVF which attaches to the façade wall [18]. The latter type of EVF [5, 9, 13, 14, 16], results in a more severe heat flux exposure of the facade surface above the opening.

2.2. Fire Engineering Design Correlations Related to EVF

There are several fire engineering design correlations available [5, 6, 9, 13, 14, 30, 32], aiming to describe the main characteristics of EVF that affect the fire safety of a building, such as the EVF height (L_L), projection (L_H), centreline temperature (T_z) and the EVF-induced heat flux to the façade ($\dot{q}''$). These semi-empirical correlations have been derived using simplified theoretical analyses in conjunction with experimental data [5, 21]. The correlations assessed in this work, grouped in three broad categories, i.e. estimation of EVF shape, average EVF gas temperature and EVF-induced heat flux to the façade, are presented in the following sections.

2.2.1. Estimation of the Main Dimensions of the EVF Envelope Estimation of the EVF shape dimensions and its thermal characteristics is mainly based on the conservation laws of mass, momentum and energy of upwards flowing jets [5, 16, 33] or, in the case of FD conditions, on temperature distribution patterns of jets without considering buoyancy and heat transfer effects [21, 30]. The EVF geometrical characteristics generally depend on the heat release rate of the fire ($\dot{Q}$), the weighted average of the opening heights (h_{eq}), the total area of vertical openings (A_v) and the external wind speed (V) [10, 33]. A range of semi-empirical correlations [5, 10, 19,

Table 1
Semi-Empirical Correlations for Estimation of the EVF Height (L_L)

Abbr.	Ref.	NoFD	FD
H1	[10]	$\max\left\{0; h_{eq}\left(2.37\left(\dfrac{\dot{Q}}{A_v \rho_{amb}\sqrt{h_{eq}}}\right)^{2/3} - 1\right)\right\}$	$1.366\left(\dfrac{1}{V}\right)^{0.43}\dfrac{\dot{Q}}{\sqrt{A_v}} - h_{eq}$
H2	[34]	$\begin{cases} 7.3\cdot 10^{-6}\left(\dfrac{\dot{Q}^{2/5}}{D_v}\right)^5, & \text{when}\quad 7.3 < \dfrac{\dot{Q}^{2/5}}{D_v} < 10.2 \\[2mm] 2.31\cdot 10^{-3}\left(\dfrac{\dot{Q}^{2/5}}{D_v}\right)^5, & \text{when}\quad 10.2 < \dfrac{\dot{Q}^{2/5}}{D_v} < 13.0 \\[2mm] 0.2\dfrac{\dot{Q}^{2/5}}{D_v}, & \text{when}\quad 13.0 < \dfrac{\dot{Q}^{2/5}}{D_v} \end{cases}$	
H3	[36]	$D_v\left(-1.02 + 0.23\dfrac{\dot{Q}^{2/5}}{D_v}\right)$	
H4	[35]	$\begin{cases} 0.0329\dfrac{\dot{Q}^{2/5}}{D_v^{2/3}}, & \text{when}\quad 11.4 < \dfrac{\dot{Q}^{2/5}}{D_v} < 16.5 \\[2mm] 0.21\dfrac{\dot{Q}^{2/5}}{D_v} & \text{when}\quad 16.5 < \dfrac{\dot{Q}^{2/5}}{D_v} \end{cases}$	
H5	[32]	$Z_n + 2l\left(\dfrac{\dot{Q}_{ex}}{\rho_{amb}c_p T_{amb}g^{1/2}l^{5/2}}\right)^{0.44}$	

21, 34–38] used to estimate EVF height (L_L) and projection (L_H) (c.f. Figure 1) are presented in Tables 1 and 2, respectively. In general, EVF height (L_L) is proportional to heat release rate ($\dot{Q}$) or excess heat release rate ($\dot{Q}_{ex}$) and inversely proportional to the effective diameter of the ventilation opening (D_v) [2, 6]. The latter quantity represents the area of the opening through which the EVF is ejected and can be estimated using Eq. (6) [6, 18]. The excess heat release rate ($\dot{Q}_{ex}$) corresponds to the fraction of the total heat release rate that is owed to combustion that takes place outside of the fire compartment. Recently [18], a correlation to estimate $\dot{Q}_{ex}$ for under-ventilated conditions has been proposed (Eq. 7); the total heat release rate ($\dot{Q}$) is assumed to be the sum of the average heat release rate at the interior of the fire compartment ($\dot{Q}_{in}$) and the excess heat release rate ($\dot{Q}_{ex}$) at the exterior; the former can be estimated using Eq. (8).

$$D_v = w_t\left(\frac{h_{eq}}{2}\right) \tag{6}$$

$$\dot{Q}_{ex} = \dot{Q} - \dot{Q}_{in} \tag{7}$$

$$\dot{Q}_{in} = 1500\, A_0\sqrt{h_{eq}} \tag{8}$$

The prescriptive methodology described in Eurocode 1 [10], which is essentially based on the correlations proposed by Law [21], allows the estimation of the maximum temperature inside the fire compartment, the dimensions and temperature profile of the EVF and the relevant convective and radiative heat fluxes. The effect of FD conditions is taken into account only in correlations H1 and P1 (Tables 1, 2), where the external wind velocity (V) is assumed to affect the fire behaviour in cases where there are openings on two opposite walls. The rest of the correlations for EVF height calculation (H2, H3 and H4) (Table 1) are mainly derived using experimental data from open air pool fires. They can also be reasonably used [33] for the determination of EVF average dimensions assuming the upper half of the opening as the fuel source; in such a case, only the convective fraction of the fire at the opening is considered. Neither compartment size nor shape has a noticeable influence on the EVF geometric characteristics [39]. A modified model for the estimation of EVF height, expressed via correlation H5, has been recently proposed [32]; in this case the characteristic length scale l is calculated using Eq. (9).

$$l = (A_0\sqrt{H_0})^{2/5} \tag{9}$$

Uncertainty in determining the EVF height (L_L) arises mainly from the different definitions of the mean or peak flame height [23, 37, 40]. Visual observations tend to yield slight overestimates of flame heights, so image processing analysis may provide more accurate results, using high frame per second analysis methodologies for the determination of flame intermittency; the latter quantity is essentially the fraction of time that part of the flame is above a certain height [23]. Since the flame is highly fluctuating, L_L is usually determined by calculating the average flame probability (intermittency). Early research [37] indicated that the fire plume above a fuel source can be divided into three main regions, characterised by the average flame probability. Using flame intermittency criteria, these three distinct regions, namely the "continuous flame", the "intermittent flame" and the "far-field plume", can be also identified in EVF [18, 41]. In this context, the flame height corresponding to the "continuous flame" ($L_{L\_0.95}$, 95% intermittency), "intermittent flame" ($L_{L\_0.50}$, 50% intermittency) and "far-field plume" ($L_{L\_0.05}$, 5% intermittency) regions can be obtained; beyond the latter region the flame cannot be seen and only hot combustion products are present. L_L can be estimated using either the 50% flame intermittency limit ($L_{L\_0.50}$), or, alternatively, by averaging the estimated flame height at the "continuous flame" ($L_{L\_0.05}$) and "far-field plume" ($L_{L\_0.95}$) regions [40]; values obtained using both methodologies are in very good agreement.

Correlations to estimate the EVF projection (L_H) are commonly based on flow analysis methodologies assuming a non-radiative heat source located at the upper half of the opening. Although some of the correlations [5, 37, 38] are derived from open air pool fire experimental data, they can also be used for the determination of EVF average dimensions by assuming the upper half of the opening as the fuel source [33]. When applying the latter correlations, one should use only the convective fraction of the heat release rate at the opening [39].

The EVF width (w_f) is commonly assumed to be equal to the opening width (w_t) [10, 21]; only scarce reports in the literature [41] indicate its dependence on

Table 2
Semi-Empirical Correlations for Estimation of the EVF Projection (L_H)

Abbr.	Ref.	NoFD	FD
P1	[10]	$\frac{h_{eq}}{3}$, when $h_{eq} \leq 1.25w_t$ $0.3h_{eq}\left(\frac{h_{eq}}{w_t}\right)^{0.54}$, when $h_{eq} > 1.25w_t$ and $w_d > 4w_t$ $0.454h_{eq}\left(\frac{h_{eq}}{2w_t}\right)^{0.54}$, in any other case	$0.605\left(\frac{V^2}{h_{eq}}\right)^{0.22}(L_L + h_{eq})$
P2	[5]	$0.13L_L$	
P3	[37]	$0.195L_L$	
P4	[38]	$0.119L_L$	

EVF height and aspect ratio of the opening (w_t/h_{eq}). It has been observed that when the fire load burns unevenly, it may result in asymmetric EVF projection and width [21]; such behaviour is not taken into account in any of the correlations currently available.

In all the aforementioned correlations, used to determine the EVF geometric characteristics, the external dimensions of the EVF are assumed to be constant in time (steady-state conditions), enabling estimation of the relevant geometrical properties using simple trigonometry rules [10, 16, 21].

2.2.2. Estimation of the EVF Centreline Temperature There is a range of correlations available to estimate the centreline temperature (T_z) of the EVF and gas products exiting through the opening [10, 21, 33]. The centreline (or flame axis) is running through the centre of the flame volume, illustrated by the dash-dotted line in the cross-sectional plane in Figure 1.

The early work of Yokoi [5] regarding the temperature distribution of upward jets emanating from a circular heat source, revealed the importance of a range of parameters, such as the equivalent radius of the opening (r_o), calculated using Eq. (10), opening height (H_o) and heat release rate ($\dot{Q}$).

$$r_0 = \sqrt{\frac{W_0(H_0 - Z_n)}{\pi}} \tag{10}$$

The effects of the thermal properties of the facade materials to the gas temperature distribution of the EVF were neglected. As soon as the plume turns upwards, ambient air entrainment becomes significant, enhancing combustion and dilution processes. Further investigation based on medium- and large-scale compartment-facade fire tests [32, 54], determined further parameters affecting the EVF temperature, such as radiative effects [33], air mass flow rate inside the compartment [32] and FD ventilation conditions [21, 31]. Investigating a broad range of semi-empirical correlations used to estimate the centreline temperatures of fire plumes and ceiling jets, Beyler [33] determined their range of applicability using uncertainty analysis. The general trend is that flame temperature is directly proportional to

Table 3
Semi-Empirical Correlations for Estimation of the EVF Centerline Temperature

Abbr.	Ref.	NoFD	FD
T1	[10]	$\left(1.0 - 0.4725\dfrac{l_x W_0}{\dot{Q}}\right)(T_0 - T_{amb})$	$\left(1.0 - 0.3325\dfrac{l_x A_0^{1/2}}{\dot{Q}}\right)(T_0 - T_{amb})$
T2	[33]	$24.6\dot{Q}^{2/3}z^{-5/3}$	
T3	[5]	$\begin{cases} 2.0\dfrac{\dot{Q}^{2/3}}{C_p^{2/3}\,\rho_{500^{\circ}C}^{2/3}\,g^{1/3}\,T_{amb}^{-1/3}(H_0 - Z_n)},\ \text{when } \dfrac{z}{r_0} \le 0.3 \\[4mm] 2.0\dfrac{\dot{Q}^{2/3}}{C_p^{2/3}\,\rho_{500^{\circ}C}^{2/3}\,g^{1/3}\,T_{amb}^{-1/3}(H_0 - Z_n)},\ \text{when } \dfrac{z}{r_0} > 0.3 \end{cases}$	
T4	[16]	$\begin{cases} 2.0\dfrac{\dot{Q}^{2/3}}{C_p^{2/3}\,\rho_{amb}^{2/3}g^{1/3}T_{amb}^{-1/3}(H_o - Z_n)},\ \text{when } \dfrac{z}{H_o - Z_n} < 0.64 \\[4mm] 1.6\dfrac{\dot{Q}^{2/3}z^{-1/2}}{C_p^{2/3}\,\rho_{amb}^{2/3}g^{1/3}T_{amb}^{-1/3}(H_o - Z_n)},\ \text{when } 0.64 \le \dfrac{z}{H_o - Z_n} \le 2.44 \\[4mm] 2.5\dfrac{\dot{Q}^{2/3}z^{-1}}{C_p^{2/3}\,\rho_{amb}^{2/3}g^{1/3}T_{amb}^{-1/3}},\ \text{when } 2.44 > \dfrac{z}{H_o - Z_n} \end{cases}$	

the distance along the centreline of the EVF, as indicated by the fundamental work of Law [21] and implemented in Eurocode 1 [10]; only this methodology accounts for the effect of ventilation conditions, proposing different correlations for NoFD and FD conditions. A more general approach was considered by Himoto [16], employing a two-dimensional analysis and experimental validation.

A range of semi-empirical correlations to estimate the EVF centreline temperature rise above the ambient temperature, $\Delta T_m = T_z - T_{amb}$, as a function of height (z) is shown in Table 3. In the majority of the investigated correlations, there is a strong dependence of the centreline temperature to the 2/3rd power of the heat release rate. The value of z used in the presented correlations corresponds either to the height above the opening lintel (T3 and T4) or the height above the virtual source (T2), estimated using the methodology proposed by Yokoi [5]. In correlation T1, the EVF centreline temperature is given as a function of the axis length from the window to the point where the calculation is made, l_x. There are various methodologies [10, 23, 33] employed to estimate the temperature of the plume at the opening of the compartment (T_o), appearing in correlation T1. In this work, the Eurocode 1 methodology [10] was employed, using Eq. (11) and (12); T_o depends on the opening area (A_o), opening width (w_t), flame length (L_f) and heat release rate ($\dot{Q}$). The EVF flame length (L_f) along the centreline is estimated using Eq. (13) and (14) for NoFD and FD conditions, respectively [10].

$$T_o = T_{amb} + \frac{520}{1 - 0.3325\left(L_f\frac{\sqrt{A_o}}{\dot{Q}}\right)}, \quad \text{when } L_f\frac{\sqrt{A_o}}{\dot{Q}} < 1 \tag{11}$$

$$T_o = T_{amb} + \frac{520}{1 - 0.4725 \left(L_f \frac{w_t}{\dot{Q}}\right)}, \quad \text{when } L_f \frac{w_t}{\dot{Q}} < 1 \tag{12}$$

$$L_f = \begin{cases} L_L + \frac{h_{eq}}{2}, & \text{when } h_{eq} \leq 1.25 w_t \text{ or if wall exists above window} \\ \left[L_L^2 + \left(L_H - \frac{h_{eq}}{3}\right)\right]^{1/2} + \frac{h_{eq}}{2}, & \text{when } h_{eq} > 1.25 w_t \text{ or if no wall exists above window} \end{cases} \tag{13}$$

$$L_f = \left(L_L^2 + L_H^2\right)^{1/2} \tag{14}$$

2.2.3. EVF-Induced Heat Flux on the Facade A range of different methodologies is available to determine the EVF-induced heat flux to external members exposed to fire. Heat flux values are mainly influenced by the compartment geometry, HRR, ambient conditions (e.g. temperature, wind speed) and interior compartment temperature [9, 10, 13, 14, 21, 22, 41].

When fire is ejecting via a compartment opening, the EVF tend to curl back, due to peripheral air entrainment, and impinge upon the wall above the opening, resulting in significant convective and radiative heat fluxes to the external surface of the façade. Recent fire events in high-rise buildings [4] indicate that the total heat flux induced by the EVF can be severe and may lead to fire propagation to adjacent floors or buildings. The EVF itself acts as a radiation source; in addition, as it evolves towards the exposed suface of the façade it imposes a convective heat flux. The facade absorbs heat from the plume and restricts the air entering through the wall side; experimental evidence suggests that increasing the width of the opening draws the fire plume closer to the wall [9].

Effective determination of fire safety requirements for external members requires accurate estimation of EVF induced heat fluxes. A range of methodologies for heat flux estimation have been proposed; generally, they are all based on the pioneering work of Law [21]. The basic principles, calculation procedures and limitations of each methodology are briefly presented here and are further analyzed in detail in Sects. 5.1–5.3. Law [21] reviewed and analysed a large number of compartment fires using cellulosic-based fire loads and formulated the heat balance for a solid surface exposed to EVF. Aiming to derive a conservative solution regarding heat transfer to external facade surfaces, she proposed a methodology that allowed estimation of convective and radiative heat fluxes due to EVF under steady-state conditions. Although this methodology has been developed in order to assess the structural integrity of external steel elements engulfed or not in flames, it can also be applied to the façade surface [15]. The heat balance for each point of a façade exposed to EVF can be expressed using Eq. (15); the convective

and radiative components can be estimated using Eq. (16) and Eq. (17), respectively.

$$\dot{q}'' = \dot{q}''_{conv} + \dot{q}''_{rad} \tag{15}$$

$$\dot{q}''_{conv} = a_c(T_z - T_{wall}) \tag{16}$$

$$\dot{q}''_{rad} = \varepsilon_z \varphi_z \sigma T_z^4 + \varphi_f \sigma T_f^4 - \sigma T_{wall}^4 \tag{17}$$

In order to employ Eqs. (16) and (17), it is necessary to estimate the convective heat transfer coefficient (a_c), the emissivity (ε) and the effective temperature of the flame (T_f). The configuration factor (φ_f) of the opening in relation to the surface depends on the size and shape of the opening and the position of the façade surface [21]; methods for estimation of the φ_f value are given in standard textbooks [10, 23]. In Eq. (17), the terms expressing the radiation from the compartment flames through the opening ($\varphi_f \sigma T_f^4$) and the radiative heat loss from the façade wall to the surroundings (σT_{wall}^4), are commonly neglected [15]. EVF thermal radiation depends strongly on the flame emissivity (ε_z), a parameter that cannot be calculated a priori for buoyant, turbulent, diffusion flames [8]. The local emissivity of the flame (ε_z) is commonly estimated using Eq. (18). A constant extinction (or emission) coefficient is usually employed ($k = 0.3$ m^{-1}) [9]; also, a constant flame thickness ($\lambda = 2L_H$) is commonly assumed, as depicted in Figure 1 (Layout I) [9, 21].

$$\varepsilon_z = 1 - \exp(-k\lambda) \tag{18}$$

By assuming that flames and hot gases exit the compartment through approximately 2/3 of the height of the opening, Eq. (19) can be used to estimate the convective heat transfer coefficient (α_c). In the original paper of Law [21], the characteristic length scale (d_{eq}), was defined as the average of the two main dimensions of the cross-section of a steel member; the characteristic length scale when referring to a point on the façade corresponds to the vertical distance between the opening sprandrel and the point itself [15]. Determination of the empirical factor c is based on experimental measurements obtained from wood crib fires conducted in medium-scale fire compartments [21]; a value of $c = 4.67$ is commonly used.

$$\alpha_c = c \left(\frac{\dot{Q}}{A_v}\right)^{0.6} \left(\frac{1}{d_{eq}}\right)^{0.4} \tag{19}$$

In the original work of Law a constant flame thickness is assumed (c.f. Figure 1, Layout I). However, it has been shown that this conservative assumption results in large errors when estimating heat fluxes at regions close to the upper part of the EVF [9]. Aiming to ameliorate this, Oleszkiewicz [9] proposed the use of a tri-

Table 4
Methodologies for Estimation of Heat Flux to the Façade

Abbr.	Radiative heat transfer		Convective heat transfer a_c (W/m²K)	Flame shape (Figure 1)
	λ_z (m)	k (m⁻¹)		
HF1	$2L_H$	0.3	Equation (19)	Layout I
HF2	Equation (20)	0.3	Equation (19)	Layout II
HF3	$2L_H$	k_{fuel} (Table 9)	Equation (19)	Layout I
HF4	$2L_H$	0.3	25	Layout I
HF5	$2L_H$	0.3	Equation (23), $1/d_{eq} = 1.0$	Layout I

angular-shaped flame (c.f. Figure 1, Layout II). This methodology [9, 26] is based on the calculation of the incident heat flux using Eq. (17), assuming a unity configuration factor. In this case, the local emissivity of the flame (ε_z) is estimated using Eq. (18) and a constant extinction coefficient, regardless of the fuel type and flame thickness. The flame thickness is estimated, assuming a triangular EVF shape [9], using Eq. (20). Equation (19) is also used to estimate the convective heat transfer coefficient, by neglecting the last term, associated with the shape of the receiving surface ($1/d_{eq} = 1.0$) [9].

$$\lambda = \frac{2L_H(L_L - z)}{L_L} \tag{20}$$

2.2.4. Estimation of EVF-Induced Heat Flux One notable feature of the various heat flux estimation methodologies is the suggested use of predefined values for the extinction (k) and convection heat transfer (α_c) coefficients, regardless of various parameters that actually affect them. In this work, the impact of such parameters, namely EVF geometry and fuel type and their effect on heat transfer components, is investigated. Aiming to establish a rigorous methodology for the estimation of the EVF-induced heat flux to external façade elements, a range of different methodologies is assessed (c.f. Table 4). Five different models, namely HF1-HF5, used for the estimation of the radiative and convective heat transfer components of the EVF-induced heat flux, are evaluated through comparison with available experimental data. In all the examined models, the total heat flux is estimated using Eq. (15), by assuming $\varphi_z = 1$ and neglecting the last two terms of Eq. (17) [9, 15]; when relevant measurements were not available, the required EVF centreline temperature (T_z) was estimated using correlation T1 [10, 21]. The effects of EVF emissivity (ε_f), extinction coefficient (k) and convective heat transfer coefficient (α_c) are investigated.

The effect of the assumed EVF geometry is initially investigated by implementing two widely applied flame shapes, i.e. an EVF with a constant flame thickness (HF1) (Figure 1, Layout I) [10, 21] and a triangular-shaped EVF (HF2) (Figure 1, Layout II) [9]. When the EVF geometry is altered, the flame thickness (λ_z) is

Table 5
Available Experimental Data and Data Collected from Each Case

Test cases	Ref.	EVF dimensions	EVF centerline temperature	Heat flux on the façade	Fuel type
8, 28	[13, 14]	✔	✔	✔	Real furniture
2, 29	[28]	✔	×	×	Wood cribs
3–7, 9–23	[9]	×	×	✔	Propane gas
30	[15]	×	×	✔	Real furniture
1, 24–27	[27]	×	×	✔	Methane gas

changed, resulting in different EVF emissivity (ε_z) values, Eq. (18). Another factor affecting the flame emissivity is the extinction coefficient (k). Although in the majority of the available literature the extinction coefficient is assumed to be constant [9, 10, 21], usually equal to 0.3 m^{-1}, in real fire scenarios this is not the case [23, 24]. In models HF1 and HF2, the extinction coefficient is valued 0.3. Aiming to investigate the effect of the extinction coefficient (k) on the estimated heat flux, different extinction coefficient values, appropriate for each fuel actually used in the respective fire test [21, 23], are employed in HF3. Finally, the impact of the convective heat transfer coefficient (α_c), using either a commonly used constant value (HF4) or a correlation taking into account the EVF height (HF5), Eqs. (19) and (23), is assessed.

3. Full-Scale Fire Compartment Experiments

Experimental data obtained in a wide range of large-scale building compartment-façade fire tests was used to evaluate available fire engineering design correlations related to EVF. The test results employed in this study cover fire tests conducted from the 1980s up to 2012 (Table 5). It is widely recognized [2, 23, 26] that even slight changes in configurations or initial conditions can very often lead to large differences in experimental results so great attention was given to the detailed collection of accurate data concerning ambient conditions, ventilation conditions and fire characteristics for each test case.

For the estimation of the EVF geometry under both NoFD and FD conditions, two experimental data sets were used [13, 14, 28]. The comprehensive data set provided by Klopovic and Turan [13, 14], based on real furniture fire tests in a compartment-façade configuration was also used for the estimation of centreline temperatures. In order to assess the available methodologies to estimate the heat flux to the façade, four sets of experimental data were used. Among them, the pioneering work of Oleszkiewicz [9] included a series of large scale NoFD compartment facade tests in a three storey facility that was used to study the impact of HRR and opening area on heat transfer to the façade at various heights from the ground. Five opening areas, ranging from 1.88 m^2 to 7.02 m^2, and four HRR values, namely 5.5 MW, 6.9 MW, 8.6 MW and 10.3 MW, were employed in the current study. More recent well documented experimental studies [13–15], under both NoFD and FD conditions, were also employed in order to account for the

Table 6
Main Characteristics of the Large-Scale Fire Tests Used in This Study

Test case	$W \times D \times H$ (m^3)	A_0 (m^2)	$A_{0,FD}$ (m^2)	Vent. cond.	$\dot{Q}$ (MW)	t (min)	GER
1	$3.0 \times 4.3 \times 1.7$	2.00×1.00	–	NoFD	2.8	5	Vent
2	$2.64 \times 3.64 \times 3.0$	2.64×1.72	–	NoFD	3.5	22	Vent
3	$5.95 \times 4.4 \times 2.75$	0.94×2.00	–	NoFD	5.5	30	Vent
4	$5.95 \times 4.4 \times 2.75$	0.94×2.70	–	NoFD	5.5	30	Vent
5	$5.95 \times 4.4 \times 2.75$	2.60×1.37	–	NoFD	5.5	30	Vent
6	$5.95 \times 4.4 \times 2.75$	2.60×2.00	–	NoFD	5.5	30	Fuel
7	$5.95 \times 4.4 \times 2.75$	2.60×2.70	–	NoFD	5.5	30	Fuel
8	$5.3 \times 3.6 \times 2.4$	2.40×1.50	–	NoFD	6.34	32	Vent
9	$5.95 \times 4.4 \times 2.75$	0.94×2.00	–	NoFD	6.9	30	Vent
10	$5.95 \times 4.4 \times 2.75$	0.94×2.70	–	NoFD	6.9	30	Vent
11	$5.95 \times 4.4 \times 2.75$	2.60×1.37	–	NoFD	6.9	30	Vent
12	$5.95 \times 4.4 \times 2.75$	2.60×2.00	–	NoFD	6.9	30	Vent
13	$5.95 \times 4.4 \times 2.75$	2.60×2.70	–	NoFD	6.9	30	Fuel
14	$5.95 \times 4.4 \times 2.75$	0.94×2.00	–	NoFD	8.6	30	Vent
15	$5.95 \times 4.4 \times 2.75$	0.94×2.70	–	NoFD	8.6	30	Vent
16	$5.95 \times 4.4 \times 2.75$	2.60×1.37	–	NoFD	8.6	30	Vent
17	$5.95 \times 4.4 \times 2.75$	2.60×2.00	–	NoFD	8.6	30	Vent
18	$5.95 \times 4.4 \times 2.75$	2.60×2.70	–	NoFD	8.6	30	Fuel
19	$5.95 \times 4.4 \times 2.75$	0.94×2.00	–	NoFD	10.3	30	Vent
20	$5.95 \times 4.4 \times 2.75$	0.94×2.70	–	NoFD	10.3	30	Vent
21	$5.95 \times 4.4 \times 2.75$	2.60×1.37	–	NoFD	10.3	30	Vent
22	$5.95 \times 4.4 \times 2.75$	2.60×2.00	–	NoFD	10.3	30	Vent
23	$5.95 \times 4.4 \times 2.75$	2.60×2.70	–	NoFD	10.3	30	Fuel
24	$3.0 \times 4.3 \times 1.7$	2.00×1.20	0.50×0.60	FD	2.8	5	Vent
25	$3.0 \times 4.3 \times 1.7$	2.00×1.20	$0.50 \times 0.60 \ (\times 4)$	FD	2.8	5	Fuel
26	$3.0 \times 4.3 \times 1.7$	2.00×1.20	0.50×0.60	FD	4.2	5	Vent
27	$3.0 \times 4.3 \times 1.7$	2.00×1.20	$0.50 \times 0.60 \ (\times 4)$	FD	4.2	5	Fuel
28	$5.3 \times 3.6 \times 2.4$	2.40×1.50	0.80×2.00	FD	5.03	32	Vent
29	$2.64 \times 3.64 \times 3.0$	2.64×1.72	0.75×1.80	FD	5.6	22	Vent
30	$3.6 \times 4.75 \times 2.45$	2.35×1.18	0.85×1.98 0.90×2.00	FD	8.8	19	Vent

effect of ventilation conditions and fuel type on the EVF characteristics, with HRR values ranging from 5.03 MW to 8.8 MW. Experimental data for a compartment fire under FD conditions (Test One) from the Dalmarnock real furniture fire test series [15] were used in this work. Data sets from the ISO13785-2 large scale façade test configuration, under both NoFD and FD conditions [27], with HRR values ranging from 2.8 MW to 4.2 MW, were also included in the current study.

The main characteristics of each experimental test case, including the compartment geometry for each configuration, ambient conditions, ventilation characteristics and fire power, are presented in detail in Table 6. Two of the most important features affecting EVF development [27], namely fuel type (Table 5) and HRR (Table 6) are presented. The impact of fuel type has been thoroughly investigated evaluating different fire sources; namely real furniture [13, 14], gas burners [9, 27] and wood cribs [28] were used to generate fires, exhibiting HRR ranging from

Table 7
Measured and Estimated Values for EVF Height, L_L (m); Numbers in Parentheses Indicate the Relative Error

Test case	2	8	28	29
Vent. cond.	NoFD	NoFD	FD	FD
Exp. data	3.1	2.78	2.03	2.2
H1	3.30 (+6.1%)	1.74 (−37.4%)	0.88 (−130.7%)	1.38 (−37.3%)
H2	2.69 (−15.2%)	3.41 (+22.7%)	2.60 (+21.9%)	1.05 (−52.3%)
H3	2.69 (−15.2%)	2.81 (+1.1%)	2.58 (+21.3%)	1.95 (−0.1%)
H4	2.19 (−41.6%)	2.30 (−17.3%)	2.09 (+2.9%)	1.60 (−27.3%)
H5	2.24 (−38.4%)	2.28 (−18.0%)	2.09 (+2.9%)	1.64 (−25.5%)

2.8 MW to 10.3 MW. Ventilation regimes for each experimental test case are also tabulated (c.f. Section 2.1); the majority of the cases are ventilation controlled (under-ventilated fire conditions).

4. Evaluation of Design Correlations

4.1. EVF Dimensions

EVF dimensions were estimated using the correlations presented in Tables 1 and 2. The effect of external wind during full scale fires has been extensively investigated by Bechtold [42] in an effort to experimentally investigate the effect of EVF on facade elements and fire spread from floor to floor through external openings. In the majority of experimental data sets available, external wind velocity is not provided. In this work, in absence of wind velocity measurements, an indicative value of 6 m/s was used, as suggested in [10, 23].

The effect of ventilation conditions on the EVF height is evident in Table 7. As expected, the façade wall is directly exposed to a more intense EVF plume in the FD cases (Test cases 28 and 29); in the NoFD test cases (Test cases 2 and 8), combustion takes place mainly at the interior of the fire compartment, thus resulting in a less intensive EVF plume that drifts further away from the façade and, therefore, exhibits a reduced impact on the façade. Under NoFD conditions, correlations H2, H3 and H4 generally under-predict experimental values, thus resulting in non-conservative estimations. In FD conditions, there is notable disagreement between experimental data and predictions when correlation H1 (Table 7) is used; the observed discrepancies are attributed to the assumed external wind velocity value of 6 m/s. The majority of the correlations avalable for the estimation of EVF height tend to under-predict experimental data, resulting in non-conservative estimations.

Good levels of agreement are observed in the estimation of the maximum projection of the EVF away from the façade (Table 8) under NoFD conditions. Nev-

Table 8
Measured and Estimated Values for EVF Projection, L_H (m); Numbers in Parentheses Indicate the Relative Error

Test case	8	28
Vent. cond.	NoFD	FD
Exp. data	0.25	1.25
P1	0.50 ($+50.0\%$)	1.64 ($+23.8\%$)
P2	0.36 (-30.6%)	0.27 (-362.9%)
P3	0.54 ($+53.7\%$)	0.40 (-215.7%)
P4	0.33 (-24.2%)	0.27 (-362.9%)
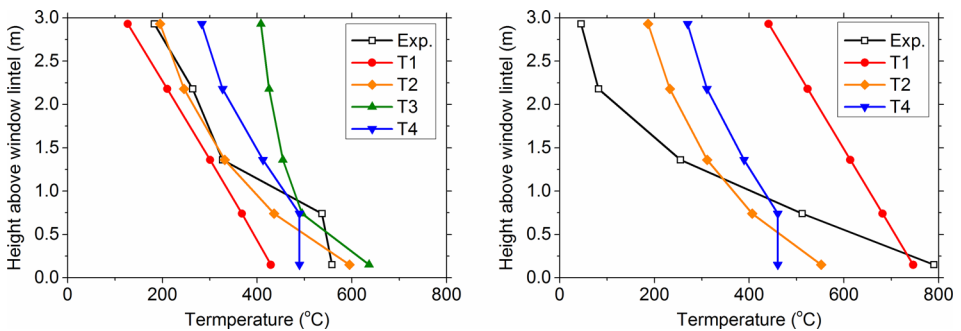
Figure 2. Vertical distribution of measured and predicted centreline EVF temperatures under NoFD (*left*) and FD (*right*) conditions.

ertheless, this is not the case for FD conditions, where all correlations, except P1, tend to significantly underestimate the experimentally determined values.

4.2. Centreline Temperature

In Figure 2, measurements of the vertical distribution of EVF centerline temperatures [13, 14] are compared to predictions obtained using correlations T1–T4 (Table 3). Determination of the virtual source and neutral plane height required for T_z is based on the assumption that the EVF emerges from the upper half of the opening, exhibiting a divergence angle of 15°, as observed during the experiments [14]. Different HRR values were used for the calculations; $\dot{Q}_{in}$ was used for correlation T1 [10], whereas a fraction of this value (27%) [14], representing the HRR outside the compartment ($\dot{Q}_{ex}$) [14, 33] was used for correlations T2, T3 and T4 [5, 16, 33].

Under NoFD conditions (Figure 2, left), correlation T1 under-predicts experimental data whereas correlations T3 and T4 [5, 16, 33], exhibit good quantitative and qualitative agreement. The point heat source assumption employed in correlation T2 [33], results in good qualitative and quantitative agreement with the experimental data. Under FD conditions (Figure 2, right), only correlation T1
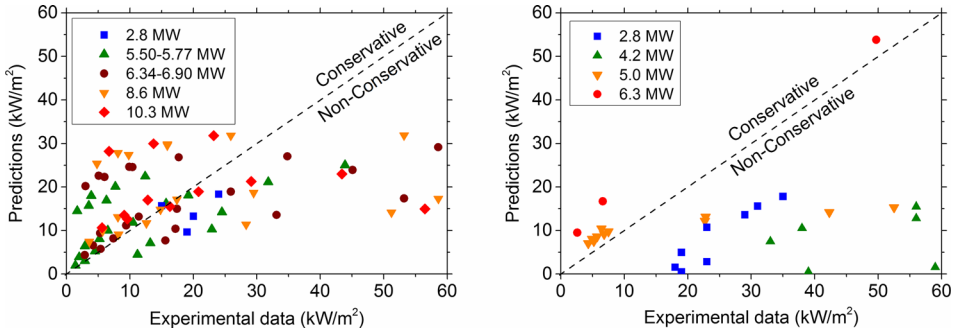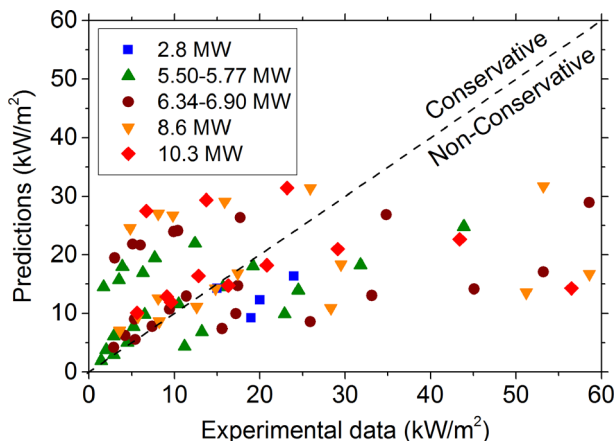
Figure 3. Experimental and predicted heat flux values (HF1) for NoFD (*left*) and FD (*right*) ventilation conditions (grouped by HRR).
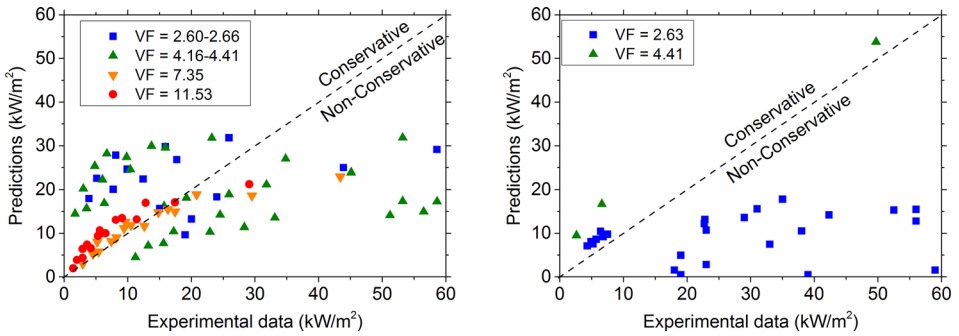
Figure 4. Experimental and predicted heat flux values (HF1) for NoFD (*left*) and FD (*right*) ventilation conditions (grouped by ventilation factor).
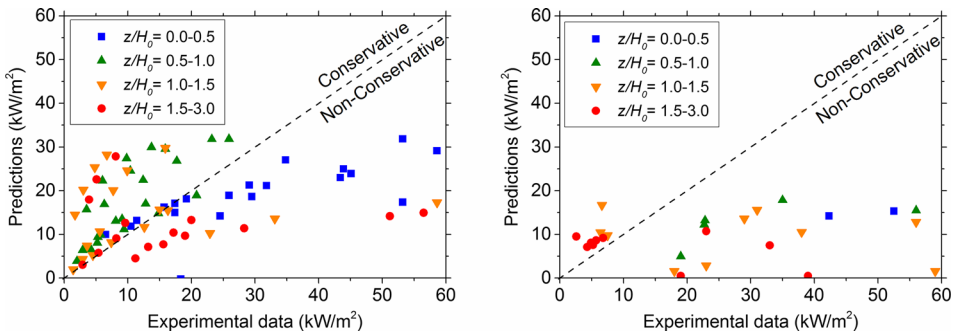
Figure 5. Experimental and predicted heat flux values (HF1) for NoFD (*left*) and FD (*right*) ventilation conditions (grouped by height).

Figure 6. Experimental and predicted heat flux values (HF2) for NoFD ventilation conditions.

estimated conservatively the temperature near the opening. Correlations originating from the experimental investigation of fire plumes (considered as upward hot jets), such as T2 and T4, significantly under-predict the EVF centerline temperature near the opening lintel.

Based on the aforementioned observations, with the exception of correlation T1 under NoFD conditions, most correlations yield mainly conservative predictions for the EVF centreline temperatures at regions far from the opening; however, non-conservative results are observed in locations close to the opening lintel.

5. Heat Flux to the Exposed Façade Surface

5.1. *Effect of EVF Shape Assumption*

In this section, the effect of shape assumption is going to be assessed, by comparing predictions of HF1 (Layout I) and HF2 (Layout II) (c.f. Table 4). Initially, predicted values of heat flux using correlation HF1 are compared to experimental measurements [9, 13–15, 27]. Aiming to determine the effect of fire power (HRR), ventilation factor (VF = $A_o H_o^{1/2}$) and height from the opening lintel (z), predictions are depicted in "groups" exhibiting similar values of HRR (Figure 3), VF (Figure 4) and non-dimensional height z/H_0 (Figure 5). It is evident that predicted values lie both in the "conservative" (over-prediction) and "non-conservative" (under-prediction) regions. Predicted values err on the safe side in roughly half of the NoFD test cases; however, the significant under-prediction of the experimental data under FD conditions may represent a potential risk when this methodology is used for building design purposes. There is no clear tendency for the effects of HRR, VF and height from the opening, Figs. 3, 4 and 5. Consequently, the results using methods HF2–HF4 are presented "grouped" only according to HRR

values. In all methods, it is generally observed that discrepancies are higher in reduced VF (Figure 4) and positions near the top of the opening (Figure 5).

Method HF2 is a modification of method HF1, by assuming a triangular flame shape (non-constant flame thickness) corresponding to Layout II (Figure 1). This methodology is applicable only for NoFD conditions [9]. Similar to predictions using HF1, there are significant discrepancies between the calculated values and measured data; though the scattering of the values is decreased, the improvement in accuracy cannot be considered significant (Figure 6). Thus, triangular EVF shape assumption does not considerably improve predicted heat flux values.

5.2. Effect of Extinction Coefficient

It is well established that radiation is the dominant mode of heat transfer in flames with characteristic length scales exceeding 1.0 m, while convection is more significant in smaller flames [26]. Accurate determination of the radiative heat transfer by the flame and gaseous combustion products is challenging since it is associated with numerous interacting physical processes, such as energy exchange between surfaces and emission and absorption by gases and particles (mainly water vapour, carbon dioxide and soot). Knowledge of the temporal and spatial distributions of EVF temperature, soot size and gas species concentrations [26], contributes to the accurate determination of radiative heat transfer; however although it is possible to estimate these parameters [43, 44], it is not practical for realistic fire scenarios. As an alternative, the use of reasonable estimates, empirical correlations or experimental measurements is commonly employed in most analytical methodologies [10, 21]. One of the main parameters influencing the radiative heat flux between a flame and an adjacent surface is the local flame emissivity (ε_z), which is generally estimated using Eq. (21) by assuming a homogeneous flame. The value of ε_z is strongly affected by the extinction coefficient of the fuel's combustion products (gases, soot) ($k_{fuel,\lambda}$) [23, 26, 43]; in general, sootier flames result in higher emissivity values.

$$\varepsilon_z = \frac{1}{\sigma T_f} \int\limits_0^\infty E_b(\lambda)\big[1 - \exp\big(-k_{fuel,\lambda}\lambda_z\big)\big]d\lambda \tag{21}$$

In recent years there has been considerable discussion on whether luminous flames can be regarded as being spectrally gray [23, 43, 44]; a range of experimental investigations [45, 46] suggest that the flame can be safely assumed to be spectrally gray for fire engineering applications. Using this assumption, Eq. (21) can be significantly simplified in the form of Eq. (22).

$$\varepsilon_z = 1 - \exp\big(-k_{fuel}\lambda_z\big) \tag{22}$$

In a real fire environment, the extinction coefficient varies both spatially and temporally, based on the prevailing local conditions, e.g. gas mixture composition and temperature, soot concentration. Evidently, an accurate estimation of the extinc-

Table 9
Extinction Coefficient or Monochromatic Absorption Coefficient for Various Fuels

Test cases	Fuel	k_{fuel} (m^{-1})	Ref.
3–7, 9–23	Propane	13.32	[23]
1, 24–27	City gas/methane	6.45	[23]
2, 29	Wood cribs	0.80	[23, 24]
8, 28, 30	Assorted furniture	1.13	[24]

tion coefficient can only be achieved by means of either extensive measurements (e.g. direct sampling of the in situ soot volume fraction) or detailed numerical simulations (e.g. use of computational fluid dynamics tools). Since such approaches are of limited value in practical fire engineering design calculations, a simplified methodology is commonly employed by using an "effective radiation temperature", assuming typical soot and gaseous concentrations for each fuel [47]. In the heat flux estimation methodology introduced by Law [21] and later modified by Oleszkiewicz [9], a constant value for the extinction coefficient (k_{fuel}) was proposed, based on available wood crib fire experimental data (c.f. Sect. 2.2.3). However, aiming to improve the accuracy of the EVF-induced heat flux estimations, the effect of using different extinction coefficient values for each fuel is investigated here. The extinction coefficient values used for each test case, based on the actual fuel employed in the respective fire test, are presented in Table 9 [21, 23, 24]. The presented values, found in the literature, are indicative and may provide practical engineering estimates. If more accurate estimations are required, a thorough numerical simulation analysis should be performed, by employing a more rigorous heat transfer methodology.

Model HF3 is a modified version of HF1, where the effect of the exact type of fuel used in each fire test is taken into account by modifying the extinction coefficient (k_{fuel}) using values presented in Table 9. The obtained predictions are shown
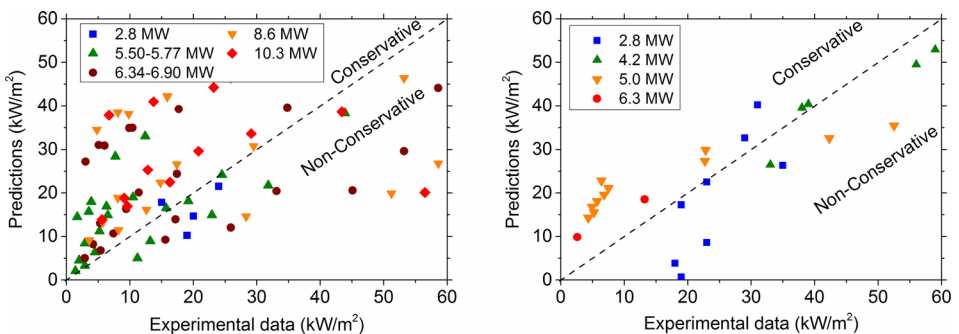
Figure 7. Experimental and predicted heat flux values (HF3) for NoFD (*left*) and FD (*right*) ventilation conditions (grouped by HRR).
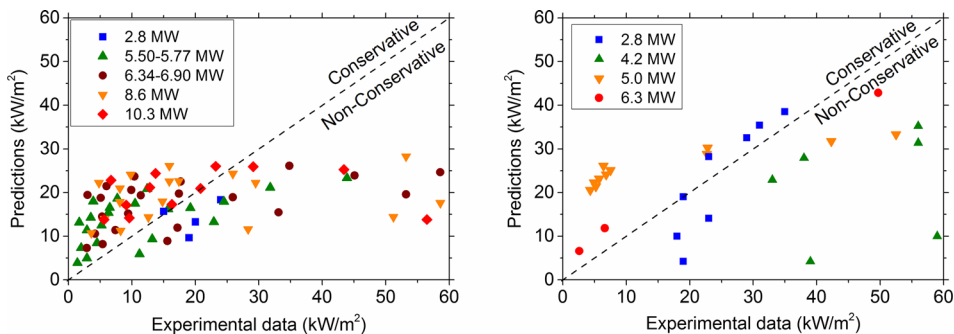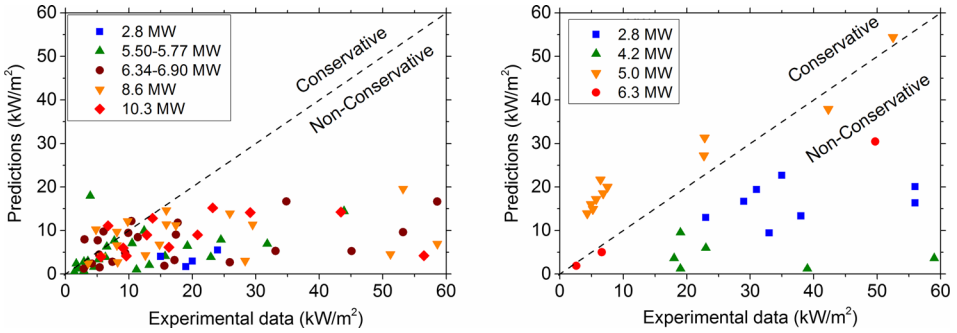
Figure 8. Experimental and predicted heat flux values (HF4) for NoFD (*left*) and FD (*right*) ventilation conditions (grouped by HRR).

in Figure 7; it is evident that method HF3 outperforms method HF1 by producing more conservative results under both NoFD and FD conditions (c.f. Figure 3). Especially under FD conditions, even at high HRR values, predicted values tend to reasonably agree with experimental data. The calculation method under NoFD conditions appears rather conservative and although the predicted values tend to be slightly lower than measured in positions near the top of the opening, they generally err on the safe side.

5.3. *Effect of Convective Heat Transfer Coefficient*

In this section, the effect of the convective heat transfer coefficient is assessed, by comparing predictions of HF4 and HF5. Convective heat transfer is usually not emphasized in most fire events, since radiation dominates heat transfer in large scale events (above 1 m in scale) [23, 48]; as a result, limited studies have focused on the determination of the convective heat transfer coefficient [48]. However, in order to effectively calculate the heat transfer rate at the boundary layer formed between the hot EVF gases and the colder façade surface, estimation of the convective heat transfer coefficient is an important parameter. In an EVF, the convective heat transfer coefficient depends on the mass flow rate and temperature of the hot gases, as well as on the temperature, size and orientation of the receiving surface [21, 23]. The convective heat transfer coefficient is obtained from relationships employing the Nusselt and Reynolds numbers, assuming a natural convective flow perpendicular to a tube or an infinite plate [9, 21].

A fixed value for the convective heat transfer coefficient, $a_c = 25$ W/(m^2 K), as suggested in Clause 3.2.2 of Eurocode 1 for external fire curves [10], is used in method HF4. Predicted results using this value produce sufficiently accurate results, Figure 8, especially under FD ventilation conditions, were larger heat flux values were observed. Results obtained for lower heat flux values, away from the opening, and for higher ventilation factors generally err on the safe side. Although method HF4 does not outperform method HF1 under NoFD conditions, predictions under FD conditions prove to be more conservative.

Figure 9. Experimental and predicted heat flux values (HF5) for NoFD (*left*) and FD (*right*) ventilation conditions (grouped by HRR).

In Clauses B.4.1 and B.4.2 of Eurocode 1 [10], the convective heat transfer coefficient is estimated using Eq. (19) and (23) for NoFD and FD conditions, respectively; values for the HRR, the opening's geometry and ventilation conditions are needed in this case. In method HF5, these equations are used to determine the convective heat transfer coefficient for each measurement position on the facade. The main difficulty in using this methodology arises in cases where the point of interest is very close to the opening, resulting in unrealistically high values of the convective heat transfer coefficient.

$$\alpha_c = 9.8 \left(\frac{\dot{Q}}{17.85 A_v} + \frac{V}{1.6} \right)^{0.6} \left(\frac{1}{d_{eq}} \right)^{0.4} \tag{23}$$

In this case, the agreement between experimental and predicted values is worse than that achieved by methods HF1 and HF4 (Figure 9). Compared to the other methodologies, predictions of HF5 are less conservative since they underestimate, in almost all cases under NoFD conditions, the measured heat flux values. Better
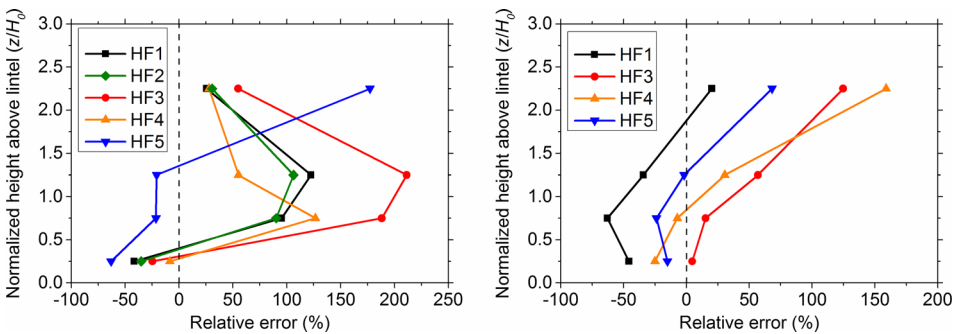
Figure 10. Relative errors of predicted heat flux values, under NoFD (*left*) and FD (*right*) conditions.

Table 10
Overall Error Evaluation Matrix for the Investigated Heat Flux Correlations

Test case	HF1 (%)	HF2 (%)	HF3 (%)	HF4 (%)	HF5 (%)	Vent. cond.
1	−25.4	−31.7	−16.0	−25.4	−81.7	NoFD
3	+139.9	+136.7	+195.8	+131.1	+68.3	NoFD
4	+316.2	+316.2	+316.4	+278.3	−20.2	NoFD
5	−50.6	−52.2	−30.9	−36.2	−81.6	NoFD
6	+22.6	+18.4	+63.6	+91.5	−52.0	NoFD
7	+78.0	+72.5	+124.9	+223.0	−27.8	NoFD
8	−43.8	−63.9	−45.7	−43.8	−83.5	NoFD
9	+123.3	+117.1	+214.6	+86.5	−14.3	NoFD
10	+239.8	+230.0	+367.9	+227.4	+48.4	NoFD
11	−54.1	−55.7	−35.5	−47.5	−83.8	NoFD
12	+5.7	+1.8	+46.3	+45.3	−57.3	NoFD
13	+50.0	+44.6	+97.9	+136.7	−35.5	NoFD
14	+74.7	+70.5	+146.9	+32.3	−32.3	NoFD
15	+163.4	+156.7	+265.1	+131.4	+16.5	NoFD
16	−70.6	−71.7	−57.4	−70.1	−89.3	NoFD
17	−8.4	−12.0	+30.9	+11.9	−62.0	NoFD
18	+59.9	+53.5	+118.0	+122.9	−28.7	NoFD
20	+106.5	+102.2	+181.3	+67.8	−11.4	NoFD
21	−81.9	−82.5	−73.1	−83.2	−93.3	NoFD
22	−7.4	−11.2	+36.5	+3.2	−60.6	NoFD
23	+36.2	+30.5	+92.1	+72.3	−36.2	NoFD
24	−51.3	–	+3.8	+14.8	−39.7	FD
25	−87.5	–	−61.7	−40.3	−74.2	FD
26	−96.3	–	−3.9	−81.4	−92.2	FD
27	−74.7	–	−4.4	−34.5	−67.8	FD
28	+142.4	–	+129.9	+73.3	−29.7	FD
30	+12.0	–	+137.9	+195.3	+133.6	FD
Average NoFD	+47.5	+42.3	+91.4	+51.9	−40.7	
Average FD	−25.9	N/A	+34.9	+51.8	−28.3	
Average ALL	+32.9	+42.3	+79.3	+51.9	−38.0	

agreement is observed under FD conditions, especially in cases exhibiting larger HRR.

5.4. Overall Analysis

An overall comparison of the façade heat flux estimation methodologies (HF1-HF5) is shown in Figure 10, where relative errors for each model are depicted as a function of the normalized height above the opening lintel (z/H_0). Due to the largely dissimilar heat flux measurement points in each of the 30 experimental test cases considered (c.f. Table 6), results have been averaged among four normalized height levels, namely 0.0–0.5, 0.5–1.0, 1.0–1.5 and 1.5–3.0. The presented estimated relative error values correspond to the normalized difference between predictions and experimental data; a positive relative error value suggests a conservative estimation, whereas a negative value signifies a potentially hazardous

Table 11
Qualitative Assessment of the Employed Methodologies for the Estimation of EVF Geometry and Thermal Characteristics

EVF characteristic	Correlation-methodology	Ref.	Main parameters	NoFD	FD
EVF height	H1	[10]	$f(h_{eq}, \dot{Q}, A_v, \rho_{amb})$	–	×
	H2	[34]	$f(\dot{Q}, D_v)$	–	–
	H3	[36]	$f(\dot{Q}, D_v)$	–	–
	H4	[35]	$f(\dot{Q}, D_v)$	×	–
	H5	[32]	$f(Z_n, l, \dot{Q}_{ex}, C_p, \rho_{amb}, g, T_{amb})$	×	–
EVF projection	P1	[10]	$f(h_{eq}, w_l)$	✔	✔
	P2	[5]	$f(L_L)$	×	×
	P3	[37]	$f(L_L)$	✔	×
	P4	[38]	$f(L_L)$	×	×
EVF centreline temperature	T1	[10]	$f(l_x, W_o, \dot{Q}, T_o, T_{amb}, A_o)$	×	✔
	T2	[33]	$f(\dot{Q}, z)$	N/A	–
	T3	[5]	$f(\dot{Q}, C_p, \rho_{500oC}, g, T_{amb}, H_o, Z_n)$	✔	N/A
	T4	[16]	$f(\dot{Q}, C_p, \rho_{amb}, g, T_{amb}, H_o, Z_n)$	–	–
EVF-induced heat flux	HF1	[10]	$\lambda_z = 2L_H, k = 0.3, \alpha_c = f(\dot{Q}, A_v, l, d_{eq})$	✔	×
	HF2	[9]	$\lambda_z = f(z), k = 0.3, \alpha_c = f(\dot{Q}, A_v, l, d_{eq})$	✔	N/A
	HF3	[23]	$\lambda_z = 2L_H, k = k_{fuel}, \alpha_c = f(\dot{Q}, A_v, l, d_{eq})$	✔	✔
	HF4	[10]	$\lambda_z = 2L_H, k = 0.3, \alpha_c = 25$	✔	✔
	HF5	[10]	$\lambda_z = 2L_H, k = 0.3, \alpha_c = f(\dot{Q}, A_v, l, d_{eq}, V)$	×	×

(✔) Conservative predictions (over-prediction), (×) non-conservative predictions (under-prediction), (–) inconsistent behaviour, (N/A) not applicable

under-prediction of the measured heat flux. All methods are found to underestimate the measured heat flux values close to the lintel opening ($z/H_0 < 0.5$). However, predictions become generally more conservative with increasing height. Method HF3 yields the most conservative results under both NoFD and FD conditions, whereas method HF1 significantly under-predicts the measured heat flux values when FD conditions prevail. The effect of the assumed flame shape is rather negligible, since predictions of HF1 and HF2 lie very close to each other. Method HF5 clearly fails in both NoFD and FD conditions, by consistently under-estimating the façade heat flux levels at low elevation values ($z/H_0 < 1.5$).

An overall evaluation of the methodologies used for the heat flux calculation is summarized in an evaluation matrix (Table 10). Relative errors are calculated for each test case and methodology, presented in details in Sects. 5.1–5.3. Average values are calculated for test cases under NoFD (Average NoFD) and FD (Average FD) ventilation conditions; an overall relative error is also calculated for all cases (Average ALL). Method HF1 is used as a "benchmark" case; predictions under NoFD conditions exhibit reasonable agreement with experimental data. However, this is not the case under FD conditions, where measurements are under-predicted, on average, by a relative error of 25.9%. The effect of flame shape is investigated only under NoFD conditions (test cases 1–23). Although, method HF2 generally outperforms method HF1, the improvement on accuracy cannot be considered significant; method HF2 over-predicts the experimental data by an overall relative error of 42%, whereas method HF1 yields an overall relative error of 47.5%. When method HF3 is implemented, by taking into account the specific fuel properties for the estimation of the extinction coefficient in the calculation of heat flux radiative component, predictions are on the safe side, under both NoFD and FD conditions. Even more conservative estimations are derived for FD conditions when method HF4 is used, where a constant value for the convective heat transfer coefficient is employed. An attempt to use a more rigorous methodology for the calculation of the convective heat transfer coefficient has not proven to be successful, as demonstrated by the large errors obtained when method HF5 is used. This can be attributed to the fact there are not clear guidelines for the application of Eqs. (19) and (23) on facades exposed to EVF. Overall, it seems that the effect of fuel properties on the extinction coefficient (c.f. Sect. 5.2) has the highest impact on façade heat flux predictions.

6. Conclusions

Acknowledging the importance of practical methodologies in filling the gap between the use of "blurry" predefined values and elaborate scientific performance-based design methodologies, this study aimed at evaluating a broad range of empirical correlations and widely employed methodologies for the estimation of EVF characteristics, using full-scale fire test data. The fundamental physical mechanisms and parameters influencing the development of EVF have been analyzed with respect to safety, emphasizing on the EVF shape and centerline temperatures. In terms of the heat flux received by the exposed side of the façade, several ana-

lytical models and correlations used to estimate the radiative and convective heat flux components have been reviewed and their limitations have been discussed. An overall qualitative assessment of the correlations and methodologies investigated in this work is presented in Table 11. Rather unexpectedly, only a small minority of the assessed correlations (e.g. P1, HF3, HF4) have resulted in conservative predictions in all the cases examined here.

Particular emphasis has been given in the estimation of the EVF dimensions and centerline temperatures, since these are the main physical parameters that affect the heat flux to the façade. Under NoFD conditions, empirical correlations for the estimation of the EVF geometric characteristics exhibited a qualitative agreement with experimental values; however, this was not the case for FD conditions, when all correlations were found to under-estimate the measured values. Regarding the EVF centreline temperature estimation, it has been demonstrated that the use of correlation T1 under-estimates experimental values under NoFD conditions, whereas it errs towards conservative estimations under FD conditions. Correlations T2, T3 and T4 may be safely used, although their accuracy in positions near the opening lintel is generally limited. The observed discrepancies may be attributed to the fact that the majority of the empirical correlations have been developed based on combustion of mainly cellulosic fuels [5, 21] or constant HRR burners [41], which do not always correspond to realistic fire scenarios.

Predictions of the heat flux to the façade, using various methodologies, under both NoFD and FD ventilation conditions, highlighted the importance of the extinction coefficient of the gaseous combustion products (k_{fuel}). It has been demonstrated that the assumption of a triangularly shaped EVF (HF2) does not affect the accuracy of the calculations. When model HF3 is used, predicted values generally err on the safe side, under both NoFD and FD conditions. In the case of FD conditions, the most conservative predictions have been obtained using model HF4, where a constant value for the convective heat transfer coefficient is employed. An attempt to use a more rigorous methodology for the calculation of the convective heat transfer coefficient has not been successful, as demonstrated by the large errors obtained when method HF5 was used. Overall, model HF3, where the effect of the fuel type used in each fire test is taken into account, has been found to outperform the other methodologies, under both FD and NoFD conditions.

Selection of a simplified fire safety engineering design methodology is determined by its intended application and by verification through detailed experimental measurements; only a method that is both versatile and practical, yielding sufficiently accurate results, may prove suitable for engineering applications. Taking into account that simplified methodologies, such as the ones presented in this work, should produce conservative design values, there is an urgent need for design guidelines that provide explicit recommendations on how to employ them. Even when more sophisticated fire safety design tools are available, a compromise is often necessary between accuracy, cost and time. Knowledge of the errors and limitations of fire engineering correlations is necessary if an analytical approach is intended to be used as an alternative to the more advanced performance-based methodologies.

Acknowledgments

References

1. Sun J, Hu L, Zhang Y (2013) A review on research of fire dynamics in high rise buildings. Theor Appl Lett 3:1–13. doi:10.1063/2.1304201
2. White N, Delichatsios M (2015) Fire hazards of exterior wall assemblies containing combustible components. Springer, New York
3. Peng L, Bu Z, Huang X (2013) Review on the fire safety of exterior wall claddings in high-rise buildings in China. Procedia Eng 62:663–670. doi:10.1016/j.proeng.2013.08.112
4. Delichatsios M (2014) Enclosure and Façade fires: Physics and applications. In: Proceedings 11th International Symposium of Fire Safety Science. University of Canterbury, New Zealand
5. Yokoi S (1960) Study on the prevention of fire spread caused by hot upward current. Building Research Institute, Report No. 34, Tokyo, Japan
6. Thomas PH (1977) Some problem aspect in fully developed room fires. Fire Standards and Safety, ASTM STP 614, A.F. Robertson, Eds., American Society for Testing and Materials, 112–130
7. Thomas PH, Heselden AJM (1972) Fully developed fires in single compartments: a cooperative research programme of the Conseil Internationale du Batiment. Conseil Internationale du Batiment Report No 20, Fire Research Note No 923
8. Thomas PH, Law M (1972) The projection of flames from burning buildings, FRN 921. Fire Research Station, Borehamwood
9. Oleszkiewicz I (1989) Heat transfer from a window fire plume to a building façade. ASME Collected papers in Heat Transfer, Book No. H00526, 123:163-170
10. EN 1991-1-2. Eurocode 1 (2002) Actions on structures, Part 1–2—General Actions—Actions on Structures Exposed to Fire. European Committee for Standardization, Brussels, Belgium
11. EN 1993-1-2. Eurocode 3 (2002) Design of steel structures, Part 1-2 – Structural fire design. European Committee for Standardization, Brussels, Belgium
12. EN 1995-1-2. Eurocode 5 (2004) Design of timber structures—Part 1–2: General—Structural fire design. European Committee for Standardization, Brussels, Belgium
13. Klopovic S, Turan OF (2001) A comprehensive study of externally venting flames, Part I: Experimental plume characteristics for through-draft and no through-draft ventilation conditions and repeatability. Fire Saf J 36:99–133. doi:10.1016/S0379-7112(00)00040-0
14. Klopovic S, Turan OF (2001) A comprehensive study of externally venting flames, Part II: Plume envelope and center-line temperature comparisons, secondary fires, wind effects and smoke management system. Fire Saf J 36:135–172. doi:10.1016/S0379-7112(00)00041-2

15. Empis CA (2010) Analysis of the compartment fire parameters influencing the heat flux incident on the structural façade. Ph.D. Thesis, University of Edinburgh, Edinburgh
16. Himoto K, Tsuchihashi T, Tanaka Y, Tanaka T (2009) Modeling thermal behaviors of window flame ejected from a fire compartment. Fire Saf J 44:230–240. doi:10.1016/j.firesaf.2008.06.005
17. Asimakopoulou E, Kolaitis D, Founti M (2013) Comparative assessment of CFD tools and the eurocode methodology in describing externally venting flames. 1st international seminar for fire safety of facades, Paris. doi:10.1051/matecconf/20130903003
18. Tang F, Hu LH, Delichatsios MA, Lu KH, Zhu W (2012) Experimental study on flame height and temperature profile of buoyant window spill plume from an under-ventilated compartment fire. Int J Heat Mass Trans 55:93–101. doi:10.1016/j.ijheatmasstransfer.2011.08.045
19. Delichatsios MA (1984) Flame heights in turbulent wall fires with significant flame radiation. Combust Sci Technol 39:195–214. doi:10.1080/00102208408923789
20. Asimakopoulou E, Kolaitis D (2015) Founti M (2016) Characteristics of externally venting flames and their effect on the façade: a detailed experimental study. Fire Technol . doi:10.1007/s10694-016-0575-5
21. Law M (1978) Fire safety of external building elements—the design approach. AISC Eng J, Second Quarter
22. Law M, O'Brien T (1981) Fire safety of bare external structural steel. Constrado, Croydon
23. Hurley MJ (2016) SFPE Handbook of fire protection engineering, 5th edn. SFPE, Quincy
24. Drysdale D (2011) An introduction in fire dynamics. Wiley, New York
25. Harmathy TZ (1979) Design to cope with fully developed fires. In: Smith EE, Harmathy TZ (eds) Design of Buildings for Fire Safety—ASTM STP 685 American Society for Testing and Materials, West Conshohocken
26. Quintiere JG (2006) Fundamentals of fire phenomena. Wiley, West Sussex
27. Yoshioka H, Ohmiya Y, Noak M, Yoshida M (2012) Large-scale façade tests conducted based on ISO 13785-2 with noncombustible façade specimens. Fire Sci Technol 31:1–22. doi:10.3210/fst.31.1
28. Lin CY (2000) Study of exposure fire spread between buildings by radiation. J Chin Inst Eng 23:493–504. doi:10.1080/02533839.2000.9670570
29. Feasey R, Buchanan A (2002) Post-flashover fires for structural design. Fire Saf J 37:83–105. doi:10.1016/S0379-7112(01)00026-1
30. Seigel LG (1969) The projection of flames from burning buildings. Fire Technol 5:43–51. doi:10.1007/BF02591612
31. Sugawa O, Momita D, Takahashi W (1997) Flow behavior of ejected fire plume from an opening effected by external side wind. Fire Saf Sci 5:249–260. doi:10.3801/IAFSS.FSS.5-249
32. Tang F, Hu LH, Delichatsios MA, Lu KH, Zhu W (2012) Experimental study on flame height and temperature profile of buoyant window spill plume from an under-ventilated compartment fire. Int J Heat Mass Transf 55:93–101. doi:10.1016/j.ijheatmasstransfer.2011.08.045
33. Beyler CL (1986) Fire plumes and ceiling jets. Fire Saf J 11:53–75. doi:10.1016/0379-7112(86)90052-4
34. Cox G, Chitty R (1985) Some source-dependent effects of unbounded fires. Combust Flame 60:219–232. doi:10.1016/0010-2180(85)90027-6
35. Hasemi Y, Tokunaga T (1984) Flame geometry effects in the buoyant plumes from turbulent diffusion flames. Fire Saf Sci Technol 4:15–26. doi:10.3210/fst.4.15

36. Heskestad G (1983) Virtual origins of fire plume. Fire Saf J 5:109–114. doi:10.1016/0379-7112(83)90003-6

37. McCaffrey BJ (1983) Momentum implications for buoyant diffusion flames. Combust Flame 52:149–156. doi:10.1016/0010-2180(83)90129-3

38. Beuther PD, George WK (1982) Measurement of the turbulent energy and temperature balances in an axisymmetric buoyant plume in a stably stratified environment. In: Proceedings 7th International Heat Transfer Conference, Munich

39. Korhonen T, Hietaniemi J (2005) Fire safety of wooden facades in residential suburb multi-storey buildings. VTT Working Papers 32

40. Audoin L, Kolb G, Torero JL, Most JM (1995) Average centreline temperatures of a buoyant pool fire obtained by image processing of video recordings. Fire Saf J 24:167–187. doi:10.1016/0379-7112(95)00021-K

41. Lee Y, Delichatsios MA, Silcock GWH (2008) Heat flux distribution and flame shapes on the inert façade. Fire Saf Sci 9:193–204. doi:10.3801/IAFSS.FSS.9-193

42. Bechtold R (1978) The role that facades play in fire spread. Fire Int 59:32–40

43. Mudan SK (1984) Thermal radiation hazards from hydrocarbon pool fires. Prog Energ Combust 10:59–80. doi:10.1205/095758297528841

44. Yuen WW, Tien CL (1977) A simple calculation scheme for the luminous flame emissivity. Proc Combust Inst 16:1481–1487. doi:10.1016/S0082-0784(77)80430-X

45. Markstein GH (1974) Radiative energy transfer from gaseous diffusion flames. Proc Combust Inst 15:1285–1294. doi:10.1016/0010-2180(76)90005-5

46. Buckius RB, Tien CL (1977) Infrared flame radiation. Int J Heat Mass Transf 20:93–106. doi:10.1016/0017-9310(77)90001-1

47. De Ris J (1979) Fire radiation—a review. Proc Combust Inst 17:1003–1016. doi:10.1016/S0082-0784(79)80097-1

48. Veloo PS, Quintiere JG (2013) Convective heat transfer coefficient in compartment fires. J Fire Sci 31:410–423. doi:10.1177/0734904113479001